PTEP

Prog. Theor. Exp. Phys. **2021**, 043F01 (11 pages)
DOI: 10.1093/ptep/ptab020

Development of highly radiopure NaI(Tl) scintillator for PICOLON dark matter search project

K. Fushimi[1,*], Y. Kanemitsu[2], S. Hirata[2,14], D. Chernyak[3], R. Hazama[4], H. Ikeda[5], K. Imagawa[6], H. Ishiura[7], H. Ito[8], T. Kisimoto[9], A. Kozlov[10], Y. Takemoto[8,11], K. Yasuda[6], H. Ejiri[12], K. Hata[5], T. Iida[13], K. Inoue[5,11], M. Koga[5,11], K. Nakamura[5,11,15], R. Orito[1], T. Shima[12], S. Umehara[12], and S. Yoshida[9]

[1]*Department of Physics, Tokushima University, 2-1 Minami Josanajima-cho, Tokushima City, Tokushima 770-8506, Japan*
[2]*Graduate School of Integrated Arts and Sciences, Tokushima University, 1-1 Minami Josanajima-cho, Tokushima City, Tokushima 770-8502, Japan*
[3]*Department of Physics and Astronomy, University of Alabama, Tuscaloosa, AL 35487, USA*
[4]*Department of Environmental Science and Technology, Osaka Sangyo University, 3-1-1 Nakagaito, Daito City, Osaka 574-8530, Japan*
[5]*Research Center for Neutrino Science, Tohoku University, 6-3 Aramaki Aza Aoba, Aobaku, Sendai City, Miyagi 980-8578, Japan*
[6]*I.S.C. Lab., 5-15-24 Torikai Honmachi, Settsu City, Osaka 566-0052, Japan*
[7]*Department of Physics, Graduate School of Science, Kobe University, 1-1 Rokkodai-cho, Nada-ku, Kobe City, Hyogo 657-8501, Japan*
[8]*Institute for Cosmic Ray Research, The University of Tokyo, 5-1-5 Kashiwanoha, Kashiwa City, Chiba 277-8583, Japan*
[9]*Department of Physics, Osaka University, 1-1 Machikaneyama-cho, Toyonaka City, Osaka 560-0043, Japan*
[10]*National Research Nuclear University "MEPhI" (Moscow Engineering Physics Institute), Moscow 115409, Russia*
[11]*Kavli Institute for the Physics and Mathematics of the Universe (WPI), 5-1-5 Kashiwanoha, Kashiwa City, Chiba 277-8583, Japan*
[12]*Research Center for Nuclear Physics, Osaka University, 10-1 Mihogaoka, Ibaraki City, Osaka 567-0042, Japan*
[13]*Faculty of Pure and Applied Sciences, University of Tsukuba, 1-1-1 Tennoudai, Tsukuba City, Ibaraki 305-8571, Japan*
[14]*Present address: Otsuka Pharmaceutical Factory, Inc., Tokushima Itano Factory, Matsunami, Itano-cho, Itano-gun, Tokushima 779-0195, Japan*
[15]*Present address: Butsuryo College of Osaka, 3-33 Ohtori Kitamachi, Nishi Ward, Sakai City, Osaka 593-8328, Japan*
[*]E-mail: kfushimi@tokushima-u.ac.jp

Received January 5, 2021; Revised February 7, 2021; Accepted February 10, 2021; Published February 16, 2021

Highly radiopure NaI(Tl) was developed to search for particle candidates of dark matter. Optimized methods were combined to reduce various radioactive impurities. ^{40}K was effectively reduced by the recrystallization method. The progenies of the decay chains of uranium and thorium were reduced by appropriate resins. The concentration of natural potassium in NaI(Tl) crystal was reduced to 20 ppb. Concentrations of alpha-ray emitters were successfully reduced by appropriate resin selection. The present concentrations of the thorium series and ^{226}Ra were

1.2 ± 1.4 μBq/kg and 13 ± 4 μBq/kg, respectively. No significant excess in the concentration of ^{210}Pb was obtained, and the upper limit was 5.7 μBq/kg at 90% CL. The achieved level of radiopurity of NaI(Tl) crystals makes the construction of a dark matter detector possible.

Subject Index F40, H20

1. Introduction

Producing a high-sensitivity radiation detector for dark matter is currently a crucial subject. Many groups are trying to find a weakly interacting massive particle (WIMP) signal by various methods and target nuclei. Although a large-volume liquid xenon (LXe) detector set stringent limits on the existence of WIMP dark matter candidates [1–3], the DAMA/LIBRA group reported a significant WIMP signal by using a highly radiopure and large-volume NaI(Tl) scintillator. They observed the annual modulating signal of the WIMP rate due to the Earth's revolution around the Sun [4]. The event rate and deposited energy of WIMPs modulate with their maximum at the beginning of June and a minimum at the beginning of December. The DAMA/LIBRA group developed a highly radiopure NaI(Tl) scintillator whose total mass was 250 kg. They reported a significant annual modulating amplitude between 2 and 6 keV$_{ee}$, where keV$_{ee}$ is the unit of energy scale calibrated by the kinetic energy of the electron [5].

Many groups are trying to verify DAMA/LIBRA's result with a NaI(Tl) scintillator [6–9]. The COSINE group started a low background measurement from 2018 with a high-purity NaI(Tl) scintillator with a total of 106 kg [8]. The event rate in the low-energy region was about 2–3 times larger than that of DAMA/LIBRA. The higher background was due to the intrinsic radioactive contamination, e.g., ^{210}Pb and ^{40}K. The beta-rays from ^{210}Pb, ^{210}Bi, and ^{40}K produce a continuous background in the energy region of interest (below 10 keV). The Compton continuum due to 1462 keV gamma-rays emitted after electron capture of ^{40}K also contributes to the background. These background events obscure the dark matter signals. Recently, COSINE reported an improved NaI(Tl) crystal, which was produced by recrystallization [10]. They proved the effectiveness of the recrystallization method to reduce the radioactive contamination in NaI(Tl).

We have tried further purification by applying a cation exchange resin, in addition to the recrystallization method. Appropriate selection of the resin enabled effective reduction of lead ions in the NaI solution. We developed an extremely high-purity NaI(Tl) crystal in which the ^{210}Pb concentration is less than 6 μBq/kg.

2. Purification methods

2.1. Recrystallization method

The recrystallization (RC) method helps to remove radioactive impurities (RIs) that are very soluble in water. The solubility of NaI in water is 75.14 at 100 °C, decreasing to 64.76 at 25 °C. The solubility is defined as the mass of solute in 100 g of water solution. The difference in the solubility between 100 °C and 25 °C enables us to obtain pure NaI sediment.

The COSINE group showed significant ^{40}K suppression with the RC method [11]. Potassium in an aqueous solution of sodium iodide forms very soluble potassium iodide (KI) or potassium hydroxide (KOH). The solubilities of KI and KOH in water are as high as 59.7 and 54.2 at 25 °C, respectively, as shown in Table 1. Since the concentration of potassium is much lower than its solubility, potassium ions remain in the water during the NaI RC process. The COSINE group reported the effectiveness of the RC method [10,11].

Table 1. The solubility of NaI, KI, KOH, and PbI_2 in water [12].

Temp. (°C)	0	20	25	100
NaI	61.54	64.1	64.76	75.14
KI	56.0	59.0	59.7	67.4
KOH	49.2	53.8	54.2	64.0
PbI_2	0.041	0.060	0.076	0.43

Table 2. The concentration of ^{nat}K and alpha-ray emitters in NaI(Tl) scintillators [13]. ^{nat}K is in ppb and others are in μBq/kg.

ID of NaI/group	^{nat}K	^{226}Ra	^{210}Pb	^{232}Th
#68	120	57 ± 7	7500	8.4 ± 2.4
#71	< 20	120 ± 10	1500	6.8 ± 0.8
#73	< 30	44 ± 7	1300	7.2 ± 0.8
#85	–	13 ± 4	< 5.7	1.2 ± 1.4
Our goal	< 20	< 100	< 10	< 10
COSINE [10]	< 42	8–60	10–420	7–35
DAMA [15]	< 20	8.7–124	10–30	2–31

We verified the effectiveness of the RC method by measuring the ^{40}K activity in NaI before and after this procedure. The activity of ^{40}K in NaI was determined using an ultra-low-background HPGe detector that is installed at the KamLAND underground facility of the Kamioka neutrino observatory. The HPGe detector was constructed by joint efforts of the Kavli IPMU (Tokyo University) and RCNS (Tohoku University) research groups. More information about the HPGe detector and underground clean room facility can be found in Refs. [13,14]. We found an apparent reduction of gamma-ray intensity with the RC method. The initial radioactivity of ^{40}K in the original (non-purified) NaI powder was in the range of 18–32 mBq/kg at 90% CL. After a single RC cycle, the activity of ^{40}K was reduced to 0.2–10 mBq/kg at 90% CL.

We prepared 100 °C NaI saturated solution in a bottle filled with pure nitrogen. The bottle was slowly cooled down to room temperature to avoid NaI crystals adhering to the bottle's surface. The NaI crystals were separated from the water solution by suction filtration. The filtration was done in a glove box flushed with pure nitrogen to prevent contact with air containing radon.

2.2. Resin method

The COSINE group reported that recrystallization worked well to reduce ^{210}Pb [10,11]. Our results also showed a significant reduction by the double and triple RC methods, as shown in Table 2. Nevertheless, we need a higher reduction to get a pure NaI(Tl) crystal below a few tens of μBq/kg. We tried to combine another strategy to remove Ra and Pb ions.

We searched extensively for the source of ^{210}Pb and found that it was not only ^{222}Rn in pure water but also ^{210}Pb in original NaI powder. We combined several methods to remove both ^{222}Rn and ^{210}Pb from the water solution of NaI. The gaseous ^{222}Rn in water was removed by bubbling the pure water with pure nitrogen gas. Longer bubbling, typically one hour, gives a significant reduction. We tried to catch Pb in the water solution of NaI by both cation exchange resin and crown ether.

Table 3. The reduction factors for concentrations of Pb ions in the NaI water solution achieved by the use of various resins.

ID	Sample	Reduction factor
1	Resin A	1/34
2	Resin B	1/64
3	Resin C	1/14
4	Resin D	1/3

We searched for the best combination of the resins by processing the NaI aqueous solution, to which was initially added 4.9 ppm of lead ion. We tested four resins, delivered by two companies. Resin A is suitable for removing strontium, uranium, and lead ions. Resin B is designed to remove lead ions. Resins C and D, delivered by a different company, are used to remove uranium and iron ions.

We measured the concentration of the Pb ion in the sample by inductively coupled plasma mass spectrometry (ICP-MS) with the Agilent 7900 at Osaka University and the Agilent 7700 at Osaka Sangyo University. The measured values of the reduction factor of the lead ion are listed in Table 3. According to the result, we selected resin B to reduce the lead ion. In addition to resin B, we apply resin A to reduce not only ^{210}Pb but also U, Ra, and Th.

2.3. Crystallization

We took the necessary precautions to avoid contact between the room's air and NaI powder during the drying process. We dried the purified NaI solution by a rotary evaporator. We selected a flask made of synthetic silica glass to avoid possible pollution from it. We filled the flask with pure nitrogen gas to break the vacuum when the drying was finished. Additional drying was done by using a vacuum oven before growing the NaI(Tl) crystal.

The large-volume NaI(Tl) crystal was produced by the Bridgman–Stockbarger technique. A high-purity graphite crucible was filled with the purified and dried NaI powder and thallium iodide. Details of the purification of the crucible material can be found in Refs. [13,14]. The crucible was installed in a quartz vessel filled with inert gas at the center of a furnace. The crucible was heated to 700 °C to melt the NaI powder, and it was slowly moved to crystallize. The crystallization takes at least two weeks of cooling and annealing to make a transparent, colorless, and large single crystal without any inclusions. The melted NaI does not interact with and infiltrate the pure graphite crucible because of the special coating on the surface of the crucible. At the end of crystal formation the NaI(Tl) ingot detaches from the crucible. We see no evidence of interaction between the crucible and melted NaI. We think that no significant pollution of the NaI(Tl) ingot occurs from the crucible material.

3. Data taking and analysis

3.1. Detector construction

The original NaI(Tl) ingot was used to make a NaI(Tl) crystal shaped as a cylinder (76.2 mm in diameter and 76.2 mm in length). An optical window made of synthetic quartz of 10 mm thickness was attached to one side of the crystal edge. The other surfaces of the crystal were covered with an enhanced specular reflector (ESR) made of polyethylene. The whole crystal was encapsulated in a 4 mm thick black acrylic container. We used an acrylic housing to minimize the absorption of low-energy gamma- and X-rays emitted by external calibration sources.

Table 4. The list of NaI(Tl) detectors and purification techniques used in their production.

Crystal ID	Purification method
#24	Resin D + radium reduction resin
#68	Resin D + cation exchange resin
#71	RC twice
#73	RC triple
#85	RC twice & resins A+B

The acrylic housing enables low-energy calibration down to 6.4 keV_{ee}. The K_β X-rays emitted after the electron capture of ^{133}Ba are between 34.9 and 35.8 keV with a total intensity of 11.5% [16]. After the photoelectronic effect on iodine, the ionized iodine emits its K_α X-rays, 28.6 and 28.3 keV [16]. If these K_α X-rays escape from the crystal, a residual energy of approximately 6.4 keV is deposited in a NaI(Tl) scintillator. This low-energy peak is useful to test the stability of the low-energy calibration.

There is a risk of moisture permeability with an acrylic housing. We tested the deliquescence when the NaI(Tl) detector was installed in the shield with pure nitrogen. The NaI(Tl) detector has not suffered any deliquescence for at least 1.8 yr.

We did several purification trials. The details of the NaI(Tl) detectors are listed in Table 4. Hereafter, we identify the NaI(Tl) detector by the crystal ID shown in Table 4.

3.2. Data acquisition system

We measured the activity of radionuclides remaining in crystals #68, #71, and #73 using an ultra-low-background setup [14] at the KamLAND underground facility. The radiopurity of two other crystals (#24 and #85) was measured in a surface laboratory at Tokushima University.

In Kamioka, the data acquisition system consists of VME-based MoGURA electronics [17] produced by Tokyo Electron Device Ltd. Several supplementary NIM modules were used to reject the majority of noise pulses from a photomultiplier tube (PMT) [13]. The MoGURA on-board flash analog-to-digital converters (FADC) can be used to record up to 10 μs long waveforms. Signal selection as well as rejection of the remaining noise pulses from the PMT were done by offline pulse shape discrimination (PSD).

In the surface laboratory, the current pulse from a PMT was divided into three routes and digitized by a CAMAC ADC [18]. One route was used for a trigger. We introduced one current signal of the PMT into a charge-sensitive ADC (CSADC: REPIC RPC-022) channel through a 200 ns cable delay. The CSADC integrates the total charge of the current pulse for 1 μs. The other current signal was introduced into the other ADC channel directly to partially integrate it.

PSD was performed to extract the alpha-ray events. The decay time of NaI(Tl) for an alpha-ray, τ_α, is 190 ns; on the other hand, that for a beta- or gamma-ray, τ_β, is 230 ns [15]. This difference enables clear discrimination of an alpha-ray and others. The parameter R was calculated as

$$R \equiv \frac{\int_{t_1}^{t_2} I(t)dt}{\int_{t_0}^{t_2} I(t)dt}, \tag{1}$$

where $I(t)$ is the input current. The upper and lower limits of the integration are defined as t_2, t_0, and t_1, respectively. The present values of t_0, t_1, and t_2 are listed in Table 5.

Table 5. Integration parameters $t_{0,1,2}$ ns in two measurement systems.

	t_0	t_1	t_2
MoGURA	0	200	1200
CAMAC	0	200	1000

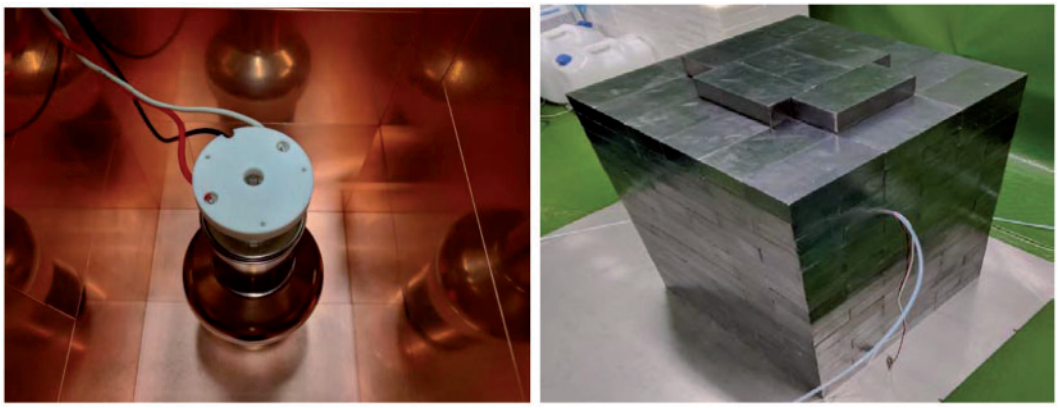

Fig. 1. The detector and the shield of the present measurement in Kamioka.

3.3. Measurement of ^{40}K in the underground laboratory

We analyzed the dependence of the concentration of ^{40}K in the NaI(Tl) detectors #68, #71, and #73 on various purification methods listed in Table 4.

We measured the concentration of ^{40}K in the NaI(Tl) crystal at Kamioka underground laboratory, Tohoku University. The ^{40}K decays by both beta decay (89.26%) and electron capture (10.72%). We need a low-background environment to measure the tiny amount of radioactivity because of the enormous external background. The Kamioka underground laboratory is suitable for reducing the background from cosmic-rays. To suppress environmental gamma-rays, the detectors were placed inside an ultra-low-background passive shielding made of 15–20 cm thick lead and 5 cm thick 99.99% pure copper layers. The structure and composition of the passive shielding have also been reported in Refs. [13,14]. Figure 1 shows crystal #73 surrounded by the copper shielding layer. An ultra-low-background PMT, Hamamatsu Photonics 4-inch R13444X [13], was attached to the optical window of the NaI(Tl) crystal by optical grease. Pure nitrogen gas was supplied into the shield to purge air containing radon.

The MoGURA data acquisition system recorded the pulse shape of the PMT output. A pulse shape discrimination was done, as shown in the left panel of Fig. 2. The energy–ratio distribution gives three loci. The PSD distribution shows the significant distortion above 4000 keV$_{ee}$ due to saturation of the PMT output. The beta-/gamma-ray energy spectrum was obtained without distortion to check the existence of the beta-ray ($E_{\beta\max} = 1311.09$ keV) and gamma-ray ($E_\gamma = 1461$ keV) [16]. We selected the beta- and gamma-ray events by PSD analysis. The energy spectra observed with crystals #68 and #71 are shown in the right panel of Fig. 2. There is a clear difference in the energy spectra between crystals #68 and #71. There is a prominent continuum below 1.3 MeV$_{ee}$ for crystal #68 due to the beta-rays of ^{40}K. The prominent beta-ray spectrum provides evidence that ^{40}K was contained in the NaI(Tl) crystal of #68. The concentration of ^{nat}K in crystal #68 was calculated as 130 ppb by a

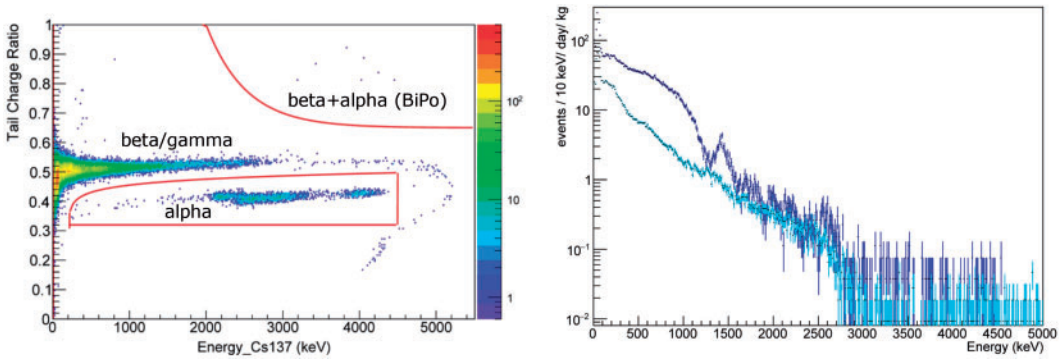

Fig. 2. Left: PSD analysis result in the case of crystal #71. Right: The energy spectra of the low-background measurement. Blue: Result with #68. Cyan: Result with #71.

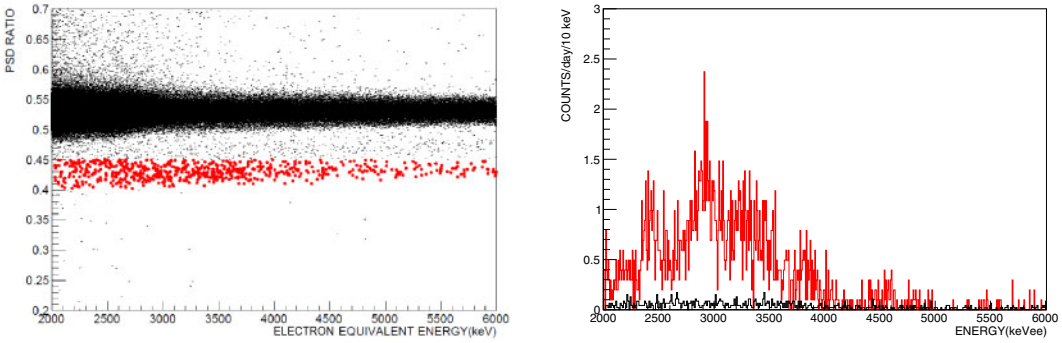

Fig. 3. Left: The PSD plot with crystal #85. The red points indicate the selected alpha-ray events. Right: Comparison between the alpha-ray energy spectra of crystal #24 (red) and crystal #85 (black).

Geant 4.10 Monte Carlo simulation, assuming that the natural abundance of ^{40}K in natural potassium is 0.0117%. On the other hand, there were no significant components of either beta- or gamma-rays from ^{40}K in the energy spectrum of crystal #71. The beta-ray event rate in crystal #71 was at least 1/6 smaller than that in crystal #68. This corresponds to the concentration of ^{nat}K being less than 20 ppb at 90% CL.

The reproducibility and the effectiveness of the triple RC method were tested by ingot #73. The upper limit of ^{nat}K was 30 ppb at 90% CL. We found that the double RC method was enough to reduce potassium contamination. We confirmed the double RC method's effectiveness with later ingots #76 and #83.

3.4. Measurement of alpha-rays in the surface laboratory

We measured the alpha concentration in purified NaI(Tl) crystals. After establishing the potassium reduction, we optimized the reduction method for alpha-ray emitters. The present crystal #85 was made by the combined method of double RC and resins. We also measured the alpha-rays in #24 to verify the reduction.

We accumulated data for live-times of 36.33 d $\times$ 1.279 kg for #85 and 11.2 d $\times$ 1.279 kg for #24. The result of the PSD analysis with crystal #85 is shown in Fig. 3. It shows the faint concentration in the region $0.4 < R < 0.45$. A large locus around $R = 0.53$ represents beta-ray, gamma-ray, and cosmic-ray events. We compared the energy spectrum of alpha-rays with that of our previous best NaI(Tl)

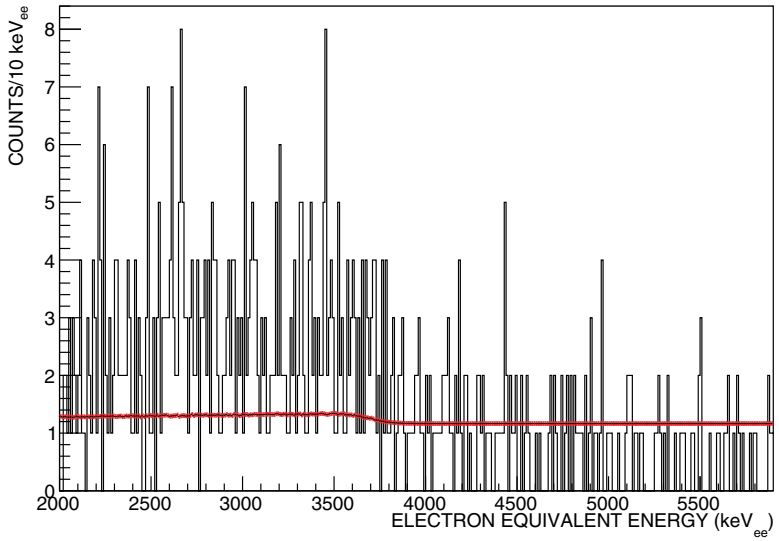

Fig. 4. The alpha-ray energy spectrum taken with crystal #85.

crystal, #24 [19]. The right panel of Fig. 3 shows the energy spectra taken with crystals #24 (red) and #85 (black). The horizontal axis shows the electron equivalent energy. There was considerable improvement in the event rate in the present work. Crystal #24 contains 163 ± 33 μBq/kg of ^{226}Ra, 149 ± 11 μBq/kg of ^{228}Th, and 86 ± 25 μBq/kg of ^{210}Pb. We analyzed the constituents of the alpha-ray spectrum of crystal #85 as described below.

The alpha-ray energy spectrum consists of two components (see Fig. 4): the lower-energy region (below 4000 keV$_{ee}$) and the higher-energy region (above 4000 keV$_{ee}$). Both components have no prominent structure. We considered that the events above 4000 keV$_{ee}$ are an accidental spread of R of high-energy cosmic-rays. We assumed that there is a constant background of cosmic-ray events below 4000 keV$_{ee}$. The energy spectrum below 4000 keV$_{ee}$ consists of constant cosmic- and alpha-rays emitted in the NaI(Tl) crystal and alpha-rays emitted on the ESR sheet.

We measured the surface concentration of alpha-ray emitters on the ESR sheet to determine the alpha-ray intensity. We applied a low-background and position-sensitive alpha-ray tracker, $\mu-$PIC [20,21]. No significant excess beyond the background was observed, as shown in Fig. 5. The upper limit of the surface contamination was calculated as 1.77×10^{-3} alpha/hr/cm^2 (90% CL).

We simulated the energy spectrum from the ESR sheet by a Geant4.10 Monte Carlo simulation [22]. We assumed that the origin of the alpha-ray was ^{210}Po because the ESR sheet attracts the progeny of ^{222}Rn. ^{210}Pb terminates the decay chain from ^{222}Rn, and the accumulated ^{210}Pb generates ^{210}Po. The red line in Fig. 4 shows the calculated energy spectrum of ^{210}Po from the ESR sheet. There is significant excess in the event rate in the low-energy region above the red line. We concluded that the excess is due to the alpha-rays emitted in the NaI(Tl) crystal.

The energy spectrum of alpha-rays from the NaI(Tl) crystal showed no prominent structure. The alpha-ray event number was too small to perform further analyses such as a time-correlation analysis. We calculated the yield by integrating the number of events instead of the peak fitting. We set the integration interval according to the alpha-ray quenching factor and energy resolution. The alpha-rays with near energies make a cluster in the energy spectrum because of the low energy resolution. The

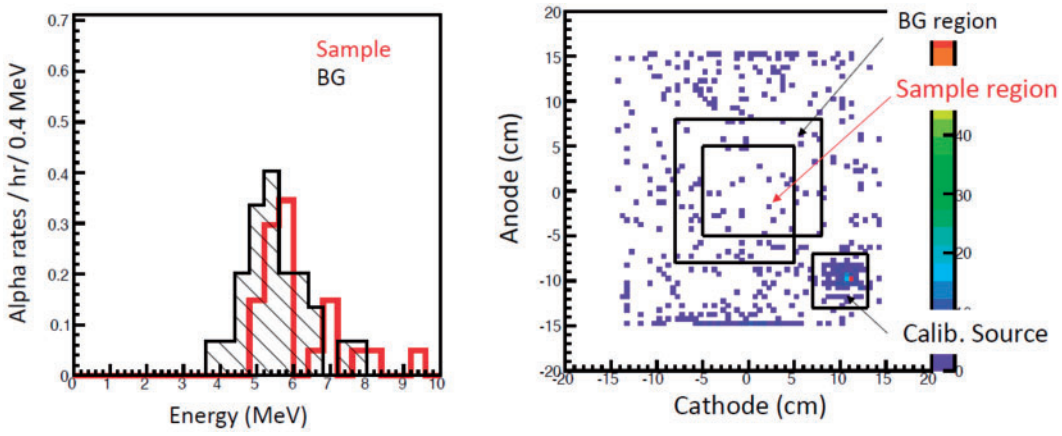

Fig. 5. Left: The energy spectra inside (red) and outside (black shaded) the sample region. Right: The distribution of emitting points of alpha-ray events. The ESR sheet is placed in the sample region.

Table 6. The RIs of alpha-ray emitters. The energy ranges (keV_{ee}) and the event numbers in the regions are listed. The detailed treatment of ^{224}Ra is described in the text.

ID	RIs	Energy range	Events
(A)	^{238}U (U), ^{232}Th (Th)	2180–2550	45 ± 10
(B)	^{234}U (U), ^{230}Th (Th), ^{226}Ra (U)	2580–2900	60 ± 11
(C)	^{228}Th (Th), ^{224}Ra* (Th), ^{222}Rn (U), ^{210}Po (U)	2970–3300	44 ± 10
(D)	^{218}Po (U), ^{212}Bi (Th), ^{224}Ra* (Th), ^{220}Rn (Th)	3300–3740	66 ± 12
(E)	^{216}Po (Th)	3820–4043	5 ± 6

alpha-ray intensity according to the clusterized energy ranges was calculated according to the alpha-ray quenching factor in the NaI(Tl) scintillator [19]. The energies listed in Table 6 are the FWHM (full width half-maximum) intervals of the clusterized peaks. The chemical symbols in parentheses indicate the decay chains of uranium and thorium. The alpha-ray electron equivalent energy, E_{ee}, is derived by

$$E_{ee} = f_\alpha E_\alpha, \tag{2}$$

where f_α is the alpha-ray quenching factor. We determined $f_\alpha = 0.58$ from the shape of the energy spectrum. The alpha-rays of ^{224}Ra lie between the (C) and (D) clusters. The alpha-rays of ^{224}Ra contribute to the event rates of both (C) and (D) because of the low energy resolution. We divided two clusters at the peak energy of the alpha-rays of ^{224}Ra. The event rates of clusters (C) and (D) contain half of the ^{224}Ra events. We confirmed the result of this analysis with the data from crystal #24. The present analysis agrees with the result by peak fitting.

The concentration of radioactivity was calculated from the event numbers in Table 6 and the total exposure 36.33 d $\times$ 1.279 kg. We have assumed that radioactivity of all isotopes in the decay chain of thorium is in secular equilibrium. The isotopes of the uranium series, ^{226}Ra, ^{222}Rn, ^{218}Po, and ^{214}Po were in secular equilibrium. We have not included ^{214}Po in the present analysis since we cannot take all the alpha-ray events from ^{214}Po. The half-life of ^{214}Po is as short as 164 μs, and the dead-time of the present data acquisition system was as long as several hundred microseconds. The concentration

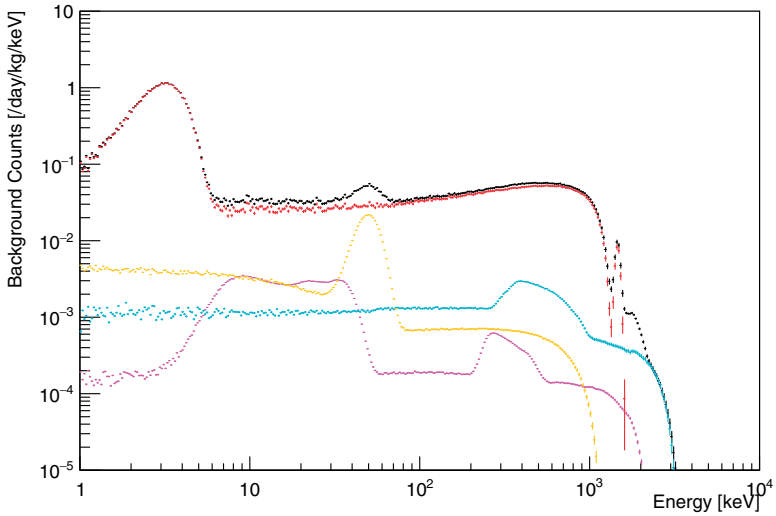

Fig. 6. The expected contribution of RIs from the NaI(Tl) crystal. Black: Total. Red: ^{40}K. Orange: ^{210}Pb and ^{210}Bi. Blue: ^{226}Ra. Magenta: Th series RIs.

of ^{218}Po was easily derived from the result of (D) as 14 ± 4 μBq/kg. That of ^{226}Ra was derived from the result of (B) as 13 ± 4 μBq/kg; both values are consistent with each other.

No significant excess was found in the concentration of ^{210}Po. We set the upper limit on the concentration as 5.7 μBq/kg at 90% CL.

4. Prospects

We have successfully developed a highly radiopure NaI(Tl) scintillator. The severe background origins, ^{40}K, ^{210}Pb, and ^{226}Ra, were successfully removed by combining the RC and resin methods. All values of radioactive impurities in crystal #85 were below our goals.

We expect highly sensitive verification of the DAMA/LIBRA experiment. A large-volume scintillator with dimensions of 12.7 cm in diameter and 12.7 cm in length is under construction. The expected energy spectra due to the intrinsic RIs are shown in Fig. 6. The next background origin is mainly gamma-rays from external RIs. They will be selected and removed by anti-coincidence of an arrayed NaI(Tl) detector system.

We will start the dark matter search experiment with large NaI(Tl) scintillators, PICOLON phase I, in the spring of 2021. It consists of at least four NaI(Tl) scintillator modules, whose total mass is 23.4 kg. We plan phases II and III with total masses of 100 and 250 kg of NaI(Tl) crystal to verify and search for new fundamental processes in nuclear and particle physics.

Acknowledgements

We acknowledge the support of the Kamioka Mining and Smelting Company. This work was supported by Japan Society for the Promotion of Science (JSPS) KAKENHI Grant Nos. 26104008, 19H00688, 20H05246, and a discretionary expense of the president of Tokushima University. This work was also supported by the World Premier International Research Center Initiative (WPI Initiative). We acknowledge Profs. H. Sekiya and A. Takeda of ICRR University of Tokyo, and Prof. Y. Takeuchi of Kobe University for continuous encouragement and fruitful discussions.

References

[1] E. Aprile et al. [XENON Collaboration], Phys. Rev. Lett. **122**, 141301 (2019).
[2] K. Abe et al. [XMASS Collaboration], Phys. Lett. B **789**, 45 (2019).
[3] D. S. Akerib et al. [LUX Collaboration], Phys. Rev. Lett. **122**, 131301 (2019).
[4] K. Freese, J. Frieman, and A. Gould, Phys. Rev. D **37**, 3388 (1988).
[5] R. Bernabei et al., Eur. Phys. J. C **73**, 2648 (2013).
[6] K.-I. Fushimi et al., J. Phys.: Conf. Ser. **1468**, 012057 (2020).
[7] J. Amaré et al., J. Phys.: Conf. Ser. **1468**, 012014 (2020).
[8] G. Adhikari et al. [COSINE-100 Collaboration], Phys. Rev. Lett. **123**, 031302 (2019).
[9] M. Antonello et al., arXiv:2012.02610 [physics.ins-det] [Search INSPIRE].
[10] B. J. Park et al., Eur. Phys. J. C **80**, 814 (2020).
[11] K. Shin, O. Gileva, Y. Kim, H. S. Lee, and H. Park, J. Radioanal. Nucl. Chem. **317**, 1329 (2018).
[12] The Chemical Society of Japan, *Kagaku Binran* (Maruzen, 1993), Handbook of Chemistry: Pure Chemistry, 4th ed. [in Japanese].
[13] A. Kozlov et al., Nucl. Instrum. Meth. Phys. Res. A **958**, 162239 (2020).
[14] A. Kozlov et al., J. Phys.: Conf. Ser. **1390**, 012118 (2019).
[15] R. Bernabei et al., Nucl. Instrum. Meth. Phys. Res. A **592**, 297 (2008).
[16] C. M. Baglin, R. B. Firestone, and S. Y. F. Chu, *Table of Isotopes* (Wiley-Interscience, New York, 1999), 8th ed.
[17] A. Terashima, Y. Takemoto, E. Yonezawa, H. Watanabe, S. Abe, and M. Nakamura, J. Phys.: Conf. Ser. **120**, 052029 (2008).
[18] K. Ichihara, K. Fushimi, N. Koori, S. Nakayama, K. Takahisa, S. Umehara, and S. Yoshida, Nucl. Instrum. Meth. Phys. Res. A **515**, 651 (2003).
[19] K. Fushimi et al., Proc. 28th Workshop Radiation Detectors and their Uses, KEK-Proceedings 2014-11 (2014) [arXiv:1407.3542 [astro-ph.IM]] [Search INSPIRE].
[20] T. Hashimoto et al., Nucl. Instrum. Meth. Phys. Res. A **977**, 164285 (2020).
[21] H. Ito, T. Hashimoto, K. Miuchi, K. Kobayashi, Y. Takeuchi, K. D. Nakamura, T. Ikeda, and H. Ishiura, Nucl. Instrum. Meth. Phys. Res. A **953**, 163050 (2020).
[22] J. Allison et al., Nucl. Instrum. Meth. Phys. Res. A **835**, 186 (2016).